pH Dependence of the Reduction of Dioxygen to Water by Cytochrome *c* Oxidase. 1. The $\mathbf{P_R}$ State Is a pH-Dependent Mixture of Three Intermediates, **A**, **P**, and **F**†

Ned Van Eps, Istvan Szundi, and Ólöf Einarsdóttir*

Department of Chemistry and Biochemistry, University of California, Santa Cruz, California 95064

Received July 19, 2002; Revised Manuscript Received January 9, 2003

ABSTRACT: Recent studies on cytochrome oxidase have indicated that the putative "peroxy" intermediate in the catalytic cycle ($\mathbf{P_R}$) is a mixture of intermediates, including **P** and **F** [Sucheta, A., et al. (1998) *Biochemistry 37*, 17905−17914], and the bench-made **P** and **F** forms appear to have the same redox state ($Fe_{a3}^{4+}{=}O^{2-}$), but a different protonation state [Fabian, M., and Palmer, G. (2001) *Biochemistry 40*, 1867−1874]. To explore the possibility that the putative $\mathbf{P_R}$ state is a pH-dependent mixture of intermediates, we investigated the reduction of dioxygen to water by the fully reduced cytochrome oxidase at pH 6.2, 7.5, and 8.5 in the visible and Soret regions (350−800 nm) using the CO flow-flash technique. Singular value decomposition and global exponential fitting of the time-resolved absorption difference spectra resolved five apparent lifetimes. The fastest three (1.5, 13, and 34 μs) were independent of pH, while the two slowest rates (80−240 μs and 1.1−2.4 ms) decreased by a factor of 2−3 as the pH increased. When the time-resolved spectra were analyzed using a unidirectional sequential model, the spectra of the reduced enzyme and the dioxygen-bound intermediate, compound **A**, were found to be pH-independent. However, the putative $\mathbf{P_R}$ intermediate was best represented by a pH-dependent mixture of compound **A**, **P**, and **F**. The ferryl form was favored at low pH. The subsequent intermediate is a ferryl with a pH-dependent electron transfer equilibrium between heme *a* and Cu_A, the reduced heme *a* being favored at low pH. These results suggest a pH-dependent reaction mechanism of the reduction of dioxygen to water by the fully reduced enzyme that is more complex than previously proposed.

Cytochrome *c* oxidase catalyzes the reduction of dioxygen to water, requiring four electrons donated by cytochrome *c* and four protons, which are taken up from the mitochondrial matrix. Four additional protons are pumped across the inner mitochondrial membrane, thus generating an electrochemical proton gradient that is used by ATP synthase to make ATP (for reviews, see refs *1* and *2*).

The details of the mechanism of the reduction of dioxygen to water by fully reduced cytochrome *c* oxidase are still not fully understood. Time-resolved resonance Raman studies have provided evidence for dioxygen binding to Fe_{a3} forming compound **A** (*3*−*5*), the presence of a ferryl intermediate (**F**),[1] and a ferric hydroxide (*6*−*9*). An additional intermediate, commonly termed the "peroxy" intermediate, $\mathbf{P_R}$, has been proposed to be generated upon decay of compound **A** and prior to the formation of **F** (*10*−*12*). However, the exact identity or even the existence of this intermediate is controversial, although it has frequently been equated with the corresponding intermediate formed during the reaction of the mixed-valence enzyme with dioxygen ($\mathbf{P_M}$) (*10*, *12*). $\mathbf{P_R}$ has also been considered to be equal to the 607 nm forms generated upon addition of hydrogen peroxide to the oxidized enzyme under alkaline conditions ($\mathbf{P_H}$) or upon exposure of the oxidized enzyme to a mixture of carbon monoxide and dioxygen ($\mathbf{P_{CO/O_2}}$). While many previous studies proposed that the O−O bond in $\mathbf{P_M}$ was intact, more recent observations have indicated that the O−O bond is already broken, and that $\mathbf{P_M}$ is in fact an oxo-ferryl state, $Fe_{a3}^{4+}{=}O^{2-}$ (*13*−*16*, *18*−*21*). The discovery of a tyrosine−histidine cross-link at the active site (*22*, *23*) led to the proposal that the tyrosine may function as an electron and a proton donor to the dioxygen bound to heme a_3, thus facilitating the cleavage of the O−O bond (*16*, *24*−*28*). Both $\mathbf{P_M}$ and $\mathbf{P_H}$ display a resonance Raman vibration at 804/768 cm^{-1} ($^{16}O_2/^{18}O_2$), attributed to $Fe_{a3}^{4+}{=}O^{2-}$ (*13*−*16*), and recent experiments in our laboratory have shown that $\mathbf{P_{CO/O_2}}$, $\mathbf{P_M}$,and $\mathbf{P_H}$ have

† This work was supported by National Institutes of Health Grant GM 53788.

* To whom correspondence should be addressed. E-mail: olof@chemistry.ucsc.edu. Phone: (831) 459-3155. Fax: (831) 459-2935.

[1] Abbreviations: Cu_A, binuclear mixed-valence copper A center; Cu_B, copper B; Fe_a, low-spin heme *a*; Fe_{a3}, heme a_3; **R***, initial Cu_B^+−CO-bound intermediate, generated following photolysis of CO from the fully reduced cytochrome *c* oxidase; **R**, fully reduced cytochrome oxidase; compound **A** (**A**), ferrous−dioxygen complex of heme a_3; $\mathbf{A_M}$, compound **A** of the mixed-valence enzyme; $\mathbf{A_R}$, compound **A** of the fully reduced enzyme; **P**, "peroxy" form of the enzyme in which heme a_3 has an absorption maximum at ∼607 nm when referenced against its oxidized state; $\mathbf{P_{CO/O_2}}$, **P** generated by exposing the oxidized enzyme to a mixture of CO and O_2; $\mathbf{P_H}$, **P** generated upon addition of H_2O_2 to the oxidized enzyme at alkaline pH; $\mathbf{P_M}$, "peroxy" intermediate formed at the binuclear center during the reaction of the mixed-valence enzyme with dioxygen; $\mathbf{P_R}$, putative "peroxy" intermediate formed at the binuclear center during the reaction of the fully reduced enzyme with dioxygen; **F**, ferryl form of the enzyme in which heme a_3 has an absorption maximum at ∼580 nm when referenced against its oxidized state; $\mathbf{F_I}$, **F** in which heme *a* is oxidized and Cu_A is reduced; $\mathbf{F_{II}}$, **F** in which heme *a* is reduced and Cu_A is oxidized; **O**, oxidized enzyme; SVD, singular value decomposition; b-spectrum, spectral changes associated with a respective first-order process.

10.1021/bi020482m CCC: $25.00
Published on Web 04/08/2003

identical absorption spectra (*17*). However, Babcock and co-workers and Rousseau and co-workers have failed to observe the 804 cm^{-1} species during the reduction of dioxygen to water by the fully reduced enzyme using time-resolved resonance Raman spectroscopy (*1*, *8*, *9*).

The exact origin of the protons that are required for the reduction of dioxygen to water and the details of the protonation state of the intermediates are still unclear. The resolution of the crystal structures of the bovine heart and *Paracoccus* cytochrome *c* oxidases revealed two major proton transfer pathways, the D-pathway and K-pathway (*23*, *29*, *30*). Spectroscopic techniques, particularly transient UV−visible spectroscopy, in combination with site-directed mutagenesis, have indicated that the D-pathway is responsible for the uptake of both scalar and translocated protons during the reduction of dioxygen to water (*31*−*33*), while proton uptake during the reduction of the oxidized enzyme has been proposed to take place through the K-pathway (*31*, *34*, *35*). However, recent studies have shown that the K-pathway may be involved during the reduction of dioxygen to water and, more specifically, during the splitting of the O−O bond and the formation of the putative $\mathbf{P_R}$ intermediate (*31*, *36*). Although these results have provided important insights into the role of the two pathways, they primarily focused on the effect of pH and selected mutations on the apparent rates of proton uptake (see ref *33* for review), while a comprehensive study on the effect of pH on the spectra of the intermediates has been lacking.

Previous studies have shown that addition of H_2O_2 to the oxidized cytochrome oxidase favors the formation of $\mathbf{P_H}$ at high pH and **F** at low pH (*18*, *20*, *37*−*41*), and recent observations have shown that the bench-made **P** form is converted to the ferryl form (**F**) upon the uptake of a proton, but without a change in redox state (*40*). The rate of conversion was found to be pH-dependent. Moreover, time-resolved optical absorption experiments in our laboratory have suggested that the intermediate formed following decay of compound **A** is not a single intermediate but rather a mixture of intermediates, including **P** and **F** (*24*). Together, these studies suggest that the composition of the putative $\mathbf{P_R}$ intermediate may be pH-dependent. To explore this possibility, we have reinvestigated the reduction of dioxygen to water at different pH values using multiwavelength detection. The results indicate that the putative $\mathbf{P_R}$ intermediate is in fact a pH-dependent mixture of three spectral forms, compound **A**, **P**, and **F**.

MATERIALS AND METHODS

Cytochrome oxidase from bovine heart was isolated according to the method of Yoshikawa et al. (*42*). The fast enzyme was prepared by the modification of the method of Hartzell and Beinert (*43*, *44*) and was generously provided by G. Liao. The fully reduced enzyme was obtained by adding sodium L-ascorbate and ruthenium hexaammine chloride to the oxidized enzyme under anaerobic conditions. The final concentrations of ascorbate and ruthenium hexaammine were 2 mM and 10 μM, respectively. Exposure of the fully reduced enzyme to CO for 1 h generated the fully reduced CO-bound enzyme.

The reaction of dioxygen with the fully reduced enzyme was followed at room temperature at different pHs using the flow-flash technique as previously described (*11*, *24*). Briefly, the fully reduced CO-bound enzyme and O_2-saturated buffer [0.1 M MES (pH 6.2), sodium phosphate (pH 7.5), and TAPS (pH 8.5)] were mixed in a 1:1 ratio in a flow apparatus interfaced with a laser photolysis/optical multichannel analyzer system (*11*). The flow cell was 5 μL in volume [10 mm (length) × 0.5 mm (width) × 1 mm (height)] and was thermostated to 298 K during the experiment. The reaction with dioxygen was initiated by photolyzing the reduced CO-bound enzyme with 532 nm laser light. The spectral changes were monitored using a pulsed xenon flash lamp.

The time-resolved optical absorption difference spectra were recorded in the visible and Soret regions on nanosecond to millisecond time scale (27−36 time delays) following CO photolysis. The spectra constitute a two-dimensional data matrix, $\Delta\mathbf{A}(\lambda_m,t_n)$, where m and n are the number of wavelengths and times collected, respectively. Singular value decomposition (SVD) of the data matrix yielded the orthonormal basis **u** vectors containing the spectral information and the **v** vectors, which describe the time dependence of the **u** vectors (*11*, *24*, *45*, *46*). The temporal **v** vectors were fit to a sum of exponential functions, which produced the apparent rates and an amplitude matrix. The latter, combined with the **u** vectors, yielded the spectral amplitudes, the so-called b-spectra, corresponding to the apparent rates (*47*). The apparent rates were assigned to the microscopic rates of a unidirectional sequential model without back reactions, and the kinetic matrix of this linear scheme was constructed (*48*). The intermediate spectra based on this unidirectional model were calculated from the experimental b-spectra and the eigenvector matrix of the kinetic matrix containing the microscopic rate constants of the unidirectional sequential scheme (*49*).

The intermediate spectra were compared to model difference spectra or the corresponding spectra observed following photolysis of the mixed-valence CO-bound enzyme in the presence of O_2. The model spectra were linear combinations of the ground state spectra of the enzyme in its various oxidation and ligation states. These include the oxidized, reduced, mixed-valence CO, and fully reduced CO-bound enzyme and the oxidized spectrum of Cu_A from *Thermus thermophilus* (*50*). The oxidized spectrum of Cu_A is very similar to the oxidized-minus-reduced spectrum of Cu_A recently reported for the bovine enzyme (*51*). The **P** and **F** forms were prepared as previously described (*20*) by exposing the oxidized enzyme to a mixture of CO and O_2 ($\mathbf{P_{CO/O_2}}$) and by the addition of hydrogen peroxide to the oxidized enzyme under acidic conditions ($\mathbf{P_H}$), respectively.

RESULTS

The time-resolved absorption difference spectra following photolysis of the fully reduced CO-bound cytochrome oxidase in the presence of oxygen were recorded in the visible and Soret regions (350−800 nm) at three pHs, 6.2, 7.5, and 8.5. The difference spectra in the visible region (480−690 nm) are shown in Figure 1. The spectra (post-minus pre-photolysis) represent 27−36 delay times, logarithmically spaced, between 100 ns and 20 ms.

While the visible difference spectra at the three pH values look similar, the apparent lifetimes obtained from SVD and the global exponential fitting are somewhat different. The

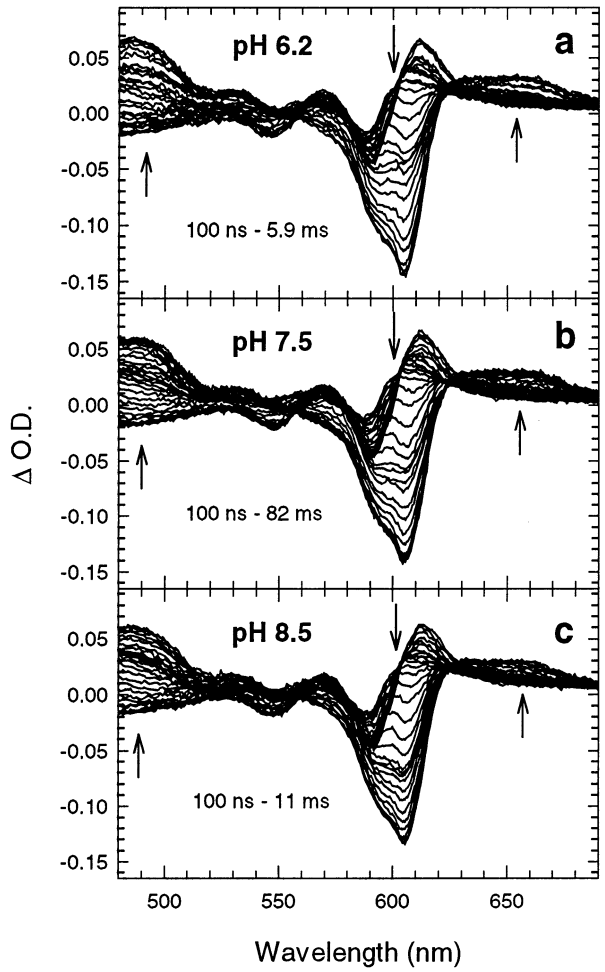

FIGURE 1: Time-resolved optical absorption difference spectra (post- minus pre-photolysis) collected in the visible region (480−690 nm) after photodissociation of the fully reduced CO-bound enzyme in the presence of dioxygen. Three data sets were collected at room temperature (25 °C) and pH 6.2 (100 ns − 5.9 ms), pH 7.5 (100 ns − 82 ms), and pH 8.5 (100 ns − 11 ms). The spectra in each data set were recorded at logarithmically spaced time delays, and each difference spectrum is an average of 40 accumulations. The effective cytochrome oxidase concentration (concentration after photolysis) was 7−8 μM. The CO and O_2 concentrations after mixing were 0.5 atm (~0.5 mM) and 625 μM, respectively.

five apparent lifetimes in the visible region were 1.5 ± 0.3 μs, 13 ± 4 μs, 34 ± 8 μs, 80 ± 20 μs, and 1.1 ± 0.2 ms at pH 6.2 and 1.5 ± 0.3 μs, 13 ± 4 μs, 39 ± 8 μs, 107 ± 20 μs, and 1.5 ± 0.2 ms at pH 7.5. Similar lifetimes were found for the data in the Soret region. The data in the visible region at pH 8.5 can also be fitted with five apparent lifetimes; however, the fourth lifetime had a large uncertainty, and any value between 100 and 260 μs was found to adequately fit the data. The five apparent lifetimes at this pH were determined on the basis of additional experiments in the near-infrared region (see below).

It is clear that only the last two lifetimes increase with an increase in pH, in agreement with previous studies (*52*−*54*). The visible spectral changes (b-spectra) associated with the apparent lifetimes at the different pH values are shown in Figure 2. The first two b-spectra ($\mathbf{b}_1$ and $\mathbf{b}_2$), attributed to the formation of the reduced (**R**) and the dioxygen-bound enzyme (compound **A**), respectively, are virtually unchanged with pH. However, there are significant spectral differences associated with the ~35 μs lifetime ($\mathbf{b}_3$), which suggests that

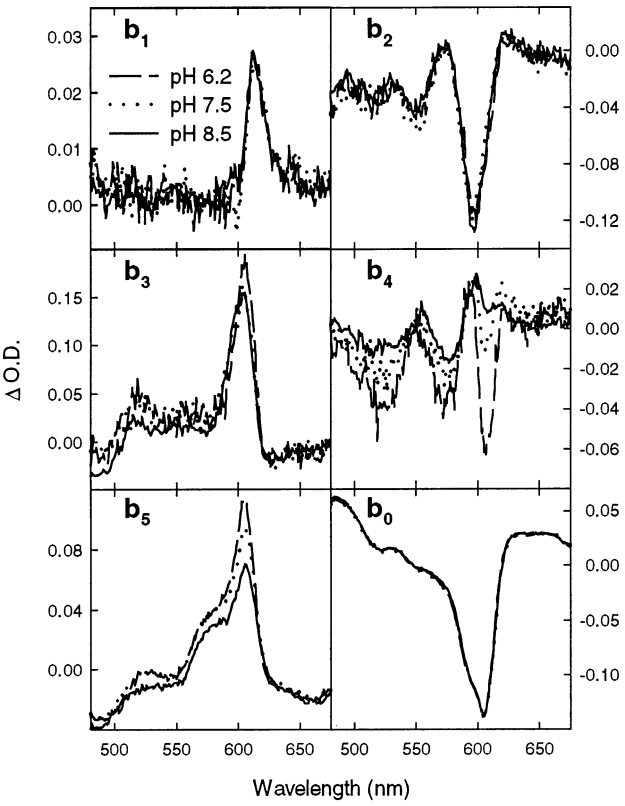

FIGURE 2: Spectral changes (b-spectra) from a five-exponential fit to each pH data set in Figure 1. The three CO flow-flash experiments were normalized for comparison purposes. For b-spectra of the pH 6.2 data set (− − −), the apparent lifetimes were 1.5 ± 0.3 μs ($\mathbf{b}_1$), 13 ± 4 μs ($\mathbf{b}_2$), 34 ± 8 μs ($\mathbf{b}_3$), 80 ± 20 μs ($\mathbf{b}_4$), and 1.1 ± 0.2 ms ($\mathbf{b}_5$). For b-spectra of the pH 7.5 data set (···), the apparent lifetimes were 1.5 ± 0.3 μs ($\mathbf{b}_1$), 13 ± 4 μs ($\mathbf{b}_2$), 39 ± 8 μs ($\mathbf{b}_3$), 107 ± 20 μs ($\mathbf{b}_4$), and 1.5 ± 0.2 ms ($\mathbf{b}_5$). For b-spectra at pH 8.5 (—), the apparent lifetimes were 1.5 ± 0.3 μs ($\mathbf{b}_1$), 13 ± 4 μs ($\mathbf{b}_2$), 36 ± 8 μs ($\mathbf{b}_3$), 240 ± 50 μs ($\mathbf{b}_4$), and 2.4 ± 0.3 ms ($\mathbf{b}_5$). The non-zero time-independent $\mathbf{b}_0$ spectrum from each experiment represents the difference spectrum extrapolated to infinite time.

the composition of the putative $\mathbf{P_R}$ intermediate, may be pH-dependent. The b-spectra associated with the fourth ($\mathbf{b}_4$) and fifth ($\mathbf{b}_5$) lifetimes, which are attributed to the formation of the ferryl (**F**) and the oxidized enzyme (**O**), respectively, are also significantly different at the three pH values.

The visible b-spectrum associated with the fourth apparent lifetime ($\mathbf{b}_4$) is rich in information and shows a number of positive and negative peaks. However, the net amplitude of the spectrum is small, particularly at pH 8.5 (Figure 2), which results in a considerable uncertainty in this lifetime. To obtain additional information about this lifetime, transient absorbance changes in the near-infrared region at 835 nm, the absorbance maximum of oxidized Cu_A, were monitored during the reduction of dioxygen to water as a function of pH (Figure 3) (*55*). The data were fit to a sum of exponential functions. At pH 6.2 and 7.5, four of the five apparent lifetimes in the visible region were confirmed (*55*). The additional 1.5 μs process observed in the visible and Soret regions was not within the time resolution of our single-wavelength detection system. At pH 8.5, we observed apparent lifetimes of 13 ± 4 μs, 36 ± 5 μs, 240 ± 50 μs, and 2.4 ± 0.3 ms. In view of the uncertainty of the fourth lifetime in the visible region and the sensitivity of the near-infrared region to changes in the redox state of Cu_A, the 240

Scheme 1: Conventional Sequential Reaction Mechanism for the Reduction of Dioxygen to Water by Cytochrome *c* Oxidase[a]

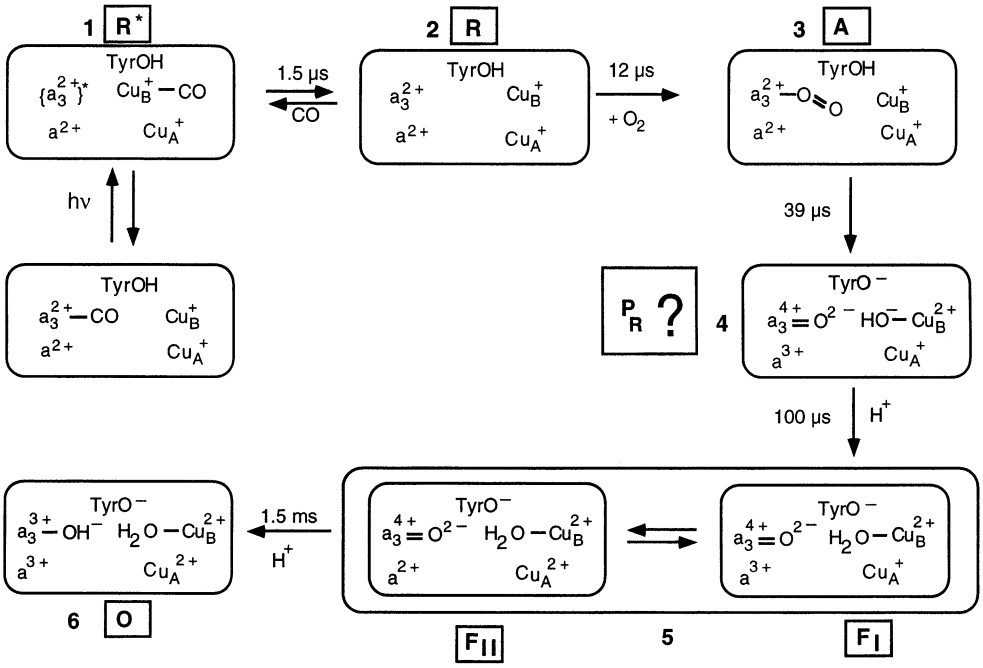

[a] The question mark associated with $\mathbf{P_R}$ serves to emphasize the fact that the structure of this intermediate has not been experimentally verified.

μs lifetime was used as the fourth lifetime in the visible region. From the combination of visible and near-infrared data, the apparent lifetimes at pH 8.5 in the visible region were 1.5 ± 0.3 μs, 13 ± 4 μs, 36 ± 8 μs, 240 ± 50 μs, and 2.4 ± 0.3 ms. The b-spectra at pH 8.5 in Figure 2 (—) correspond to these lifetimes. Similar lifetimes were used to fit the data in the Soret region.

Kinetic Modeling. While SVD and global exponential fitting provide the b-spectra and apparent lifetimes directly from the experimental data, a mechanism with associated microscopic rate constants for extracting the spectra of the intermediates has to be proposed. Scheme 1 shows a minimal unidirectional sequential mechanism, the intermediates of which are consistent with earlier proposed models (*10*−*12*). The structure of heme a_3 in intermediate **4** is displayed as ferryl, and the reducing equivalent and proton required to break the dioxygen bond are shown to arise from heme *a* and tyrosine, respectively. However, the question mark associated with intermediate **4** serves to emphasize the fact that the structure of this intermediate has not been experimentally verified. Intermediate **5** is observed as a single species, but truly represents a redox equilibrium between heme *a* and Cu_A, denoted by $\mathbf{F_I}$ and $\mathbf{F_{II}}$.

*Intermediates **1** (**R***), **2** (**R**), and **3** (Compound **A**)*. One of the primary criteria for the validity of a proposed mechanism is a good agreement between the extracted spectra and model spectra of the intermediates. Model spectra of intermediate **1** (**R***) and compound **A** cannot be made on the bench since these intermediates are only formed transiently. We have previously shown that the extracted spectrum of intermediate **2** (**R**) is in good agreement with that of the fully reduced enzyme (*11*, *46*). Furthermore, we have recently shown that the spectra of compound **A** formed during the reaction of the mixed-valence and the fully reduced cytochrome oxidase with dioxygen are identical in both the visible and Soret regions at room temperature (*17*).

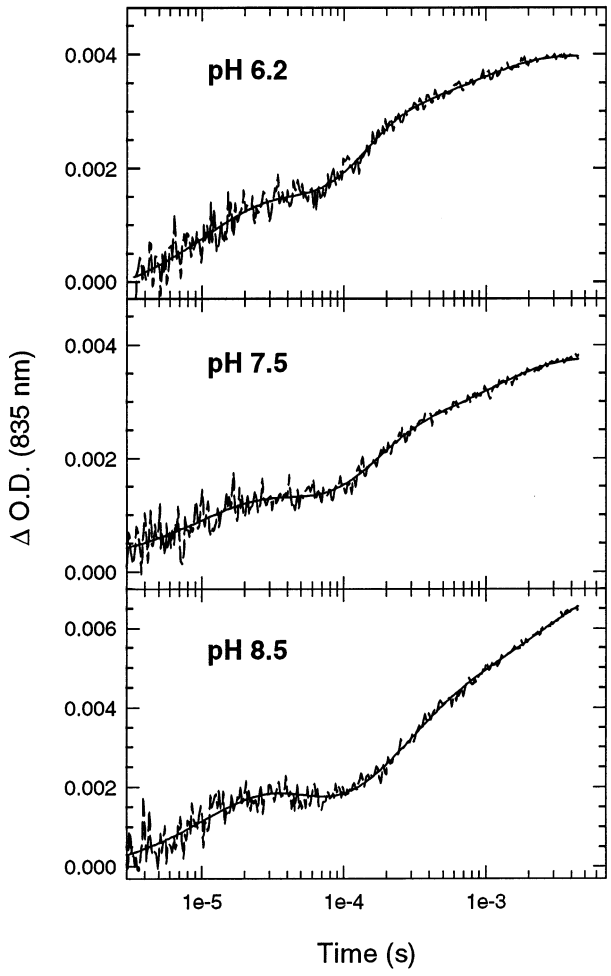

FIGURE 3: Transient absorbance changes at 835 nm following photolysis of the fully reduced CO-bound enzyme in the presence of dioxygen at pH 6.2, 7.5, and 8.5. The solid lines superimposed on the data represent a four-exponential fit to the data.

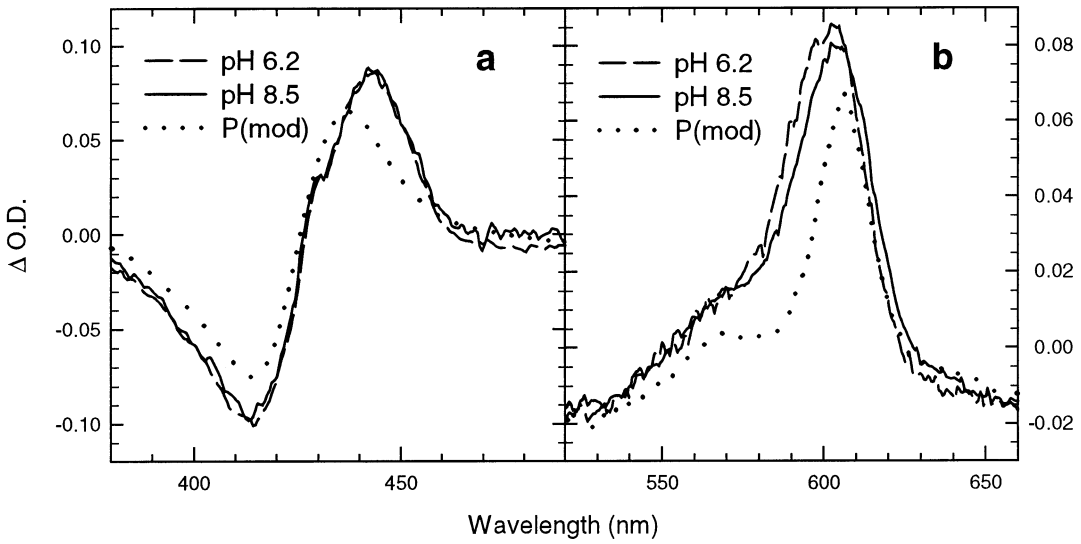

FIGURE 4: Experimental difference spectra of intermediate **4** ($\mathbf{P_R}$) at pH 6.2 (− − −) and 8.5 (—). The spectra are referenced vs the oxidized enzyme and were extracted using a sequential unidirectional mechanism (Scheme 1). The model difference spectrum, $\mathbf{P_{CO/O_2}}$, generated by exposing the oxidized enzyme to CO in the presence of O_2, is shown for comparison (···).

This is in agreement with previous studies at cryogenic temperatures (*56*−*58*). The spectra of intermediates **R*** and **R** and compound **A** extracted from our time-resolved data at the different pHs using Scheme 1 were found to be independent of pH (not shown).

Intermediate 4. The primary question concerns the nature of intermediate **4**, i.e., whether it is equal to $\mathbf{P_M}$. Figure 4 shows the spectrum of intermediate **4** in the Soret and visible regions at pH 6.2 (− − −) and 8.5 (—) extracted from the transient data using the mechanism in Scheme 1. The reference spectrum is that of the fully oxidized enzyme. The dotted lines represent the model spectrum of **P** generated by exposing the oxidized enzyme to CO in the presence of O_2 ($\mathbf{P_{CO/O_2}}$). The low-spin heme *a* is oxidized in the model compound. The oxidized spectrum of Cu_A has been subtracted from the model spectrum to match the redox state of Cu_A in intermediate **4** (Scheme 1). It is clear that there are significant spectral differences between the extracted spectrum of intermediate **4** and the $\mathbf{P_{CO/O_2}}$ model spectrum in both spectral regions, in support of our previous studies (*17*). We have recently shown that the spectrum of **P** generated by exposing the oxidized enzyme to CO in the presence of O_2 is equivalent to the spectrum of the species formed during the reaction of the mixed-valence enzyme with dioxygen ($\mathbf{P_M}$) and the spectrum of the **P** form generated by the addition of hydrogen peroxide to the oxidized enzyme at alkaline pH, $\mathbf{P_H}$ (*17*). Thus, these results provide solid evidence that the spectrum of intermediate **4** is not equivalent to that of $\mathbf{P_M}$.

Figure 4 shows that the visible difference spectrum of the putative $\mathbf{P_R}$ intermediate is different at pH 6.2 and 8.5, with the pH 6.2 spectrum being significantly broader on the blue side of the absorption maximum but narrower on the red side. There are also large spectral differences between the spectra of intermediate **4** at pH 6.2 and 8.5 and the bench-made **P** in the Soret region. Figure 5 shows the difference spectrum of intermediate **4** in the visible region at three different pH values when referenced against the fully reduced CO-bound enzyme. It is clear that the spectra of intermediate **4** vary with pH, with the largest difference centered at ∼595 nm. This suggests that the spectrum of intermediate **4** may contain a spectral contribution from compound **A**. The spectrum at pH 6.2 is also significantly different from that at pH 7.5 and 8.5 in the spectral region between 620 and 650 nm.

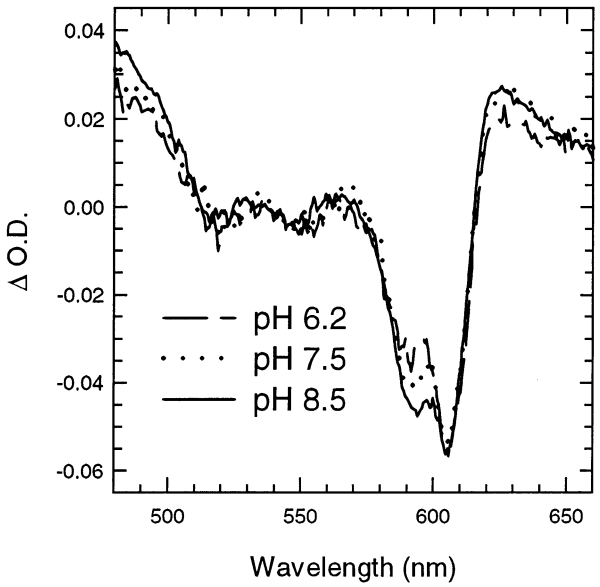

FIGURE 5: Visible experimental difference spectra of intermediate **4** ($\mathbf{P_R}$), referenced vs the fully reduced CO-bound enzyme at pH 6.2 (− − −), 7.5 (···), and 8.5 (—). The spectra were extracted from the time-resolved optical absorption visible data using a unidirectional sequential mechanism (Scheme 1).

Figure 6 (—) shows the difference between intermediate **4** ($\mathbf{P_R}$) and **A** at pH 7.5 in the visible region. The difference spectrum is best modeled by 33% of the bench-made **P** and 34% of **F** minus 67% of compound **A** [Figure 6 (− − −)]. Therefore, compound **A** is converted into both **P** and **F**. However, it is only partially converted (67%), which suggests that compound **A** contributes to the spectrum of intermediate **4**.

Intermediate 5. Scheme 1 shows that intermediate **5** represents the redox equilibrium between heme *a* and Cu_A. The two species are denoted $\mathbf{F_I}$ and $\mathbf{F_{II}}$. Figures 7 and 8

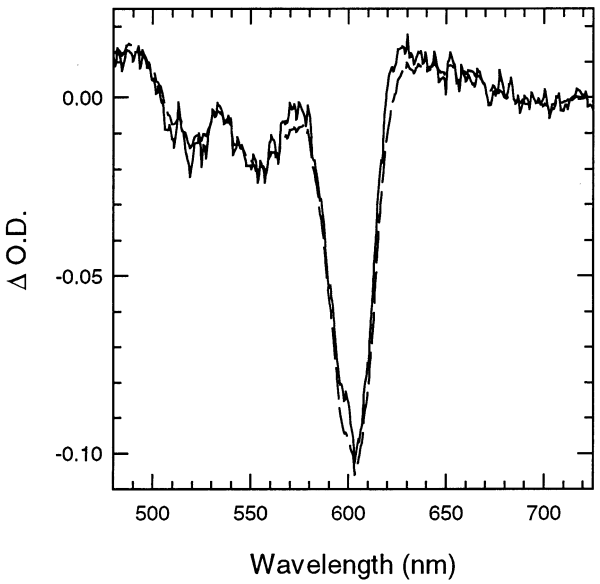

FIGURE 6: Difference between the experimental spectrum of intermediate **4** ($\mathbf{P_R}$) and the experimental spectrum of compound **A** in the visible region at pH 7.5 (—). Both spectra were extracted using a unidirectional sequential mechanism. The model difference spectrum (— — —) represents the following percentages of the respective model spectra: 34% $\mathbf{P_{CO/O_2}}$ + 33% **F** − 67% **A**.

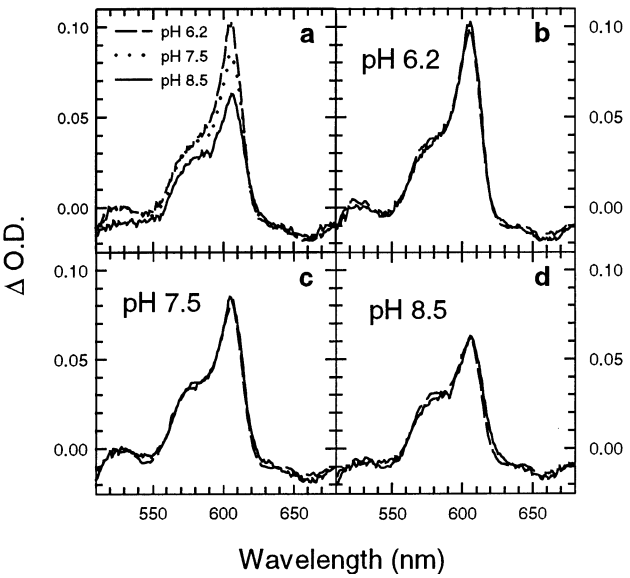

FIGURE 7: (a) Visible spectra of intermediate **5** ($\mathbf{F_I}$/$\mathbf{F_{II}}$), referenced against the oxidized enzyme, at three pHs (6.2, 7.5, and 8.5). The spectra were extracted from the time-resolved data using a unidirectional sequential mechanism. (b−d) Individual experimental difference spectra of intermediate **5** (—) at pH 6.2, 7.5, and 8.5, respectively. The model difference spectrum (— — —) is made up of 32% $\mathbf{F_I}$ + 68% $\mathbf{F_{II}}$ at pH 6.2, 44% $\mathbf{F_I}$ + 56% $\mathbf{F_{II}}$ at pH 7.5, and 50% $\mathbf{F_I}$ + 40% $\mathbf{F_{II}}$ + 10% $\mathbf{P_{CO/O_2}}$ at pH 8.5.

(panel a) show the spectrum of intermediate **5** at the three different pH values referenced against the spectrum of the oxidized enzyme. It is clear that the spectra in both the visible and Soret regions are significantly pH-dependent. Figures 7 and 8 (panels b−d) show the modeling of the Soret and visible spectra of intermediate **5** at the three pH values using a mixture of $\mathbf{F_I}$ and $\mathbf{F_{II}}$. The model spectrum of **F** was generated by adding H_2O_2 to the oxidized enzyme at acidic pH (*20*), and the spectra of $\mathbf{F_I}$ and $\mathbf{F_{II}}$ were obtained by adding the reduced-minus-oxidized spectra of Cu_A and heme

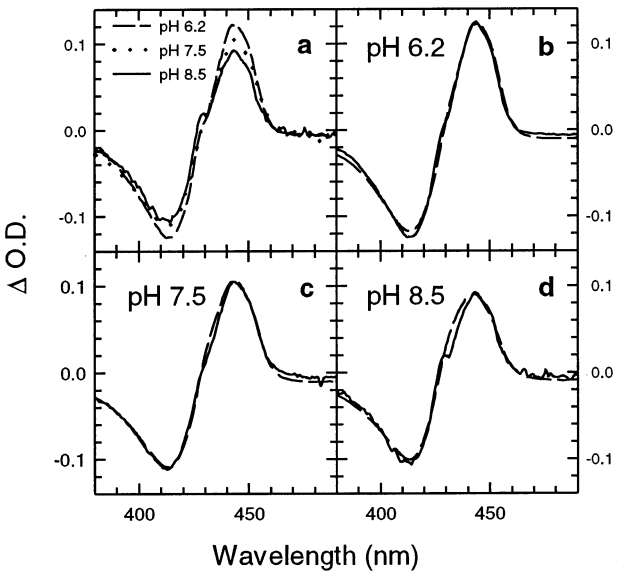

FIGURE 8: (a) Soret spectra of intermediate **5** ($\mathbf{F_I}$/$\mathbf{F_{II}}$), referenced against the oxidized enzyme, at three pHs (6.2, 7.5, and 8.5). The spectra were extracted from the time-resolved data using a unidirectional sequential mechanism. (b−d) Individual experimental difference spectra of intermediate **5** (—) at pH 6.2, 7.5, and 8.5, respectively. The model difference spectrum (— — —) is made up of 30% $\mathbf{F_I}$ + 70% $\mathbf{F_{II}}$ at pH 6.2, 45% $\mathbf{F_I}$ + 55% $\mathbf{F_{II}}$ at pH 7.5, and 50% $\mathbf{F_I}$ + 40% $\mathbf{F_{II}}$ + 10% $\mathbf{P_{CO/O_2}}$ at pH 8.5.

a, respectively, to the spectrum of **F**. It is clear that at pH 6.2, the equilibrium is significantly shifted toward $\mathbf{F_{II}}$, while at pH 8.5, it is slightly shifted toward $\mathbf{F_I}$. Interestingly, a small contribution of $\mathbf{P_{CO/O_2}}$ is required to adequately model the spectrum at pH 8.5.

DISCUSSION

The unidirectional sequential scheme (Scheme 1) has most commonly been used to describe the reaction mechanism of cytochrome oxidase because of its simplicity and because it is one of the few kinetic schemes that allows the calculation of intermediate spectra from the experimental b-spectra without any further assumptions. For a sequential unidirectional scheme, the kinetic problem is mathematically well determined and allows the direct and accurate calculation of the spectra of the pure sequential states even if the reaction rates are close and the concentrations of the intermediates overlap in time (*49*). A comparison between these intermediate spectra and model spectra, which are linear combinations of the ground-state spectra of the enzyme in its various oxidation and ligation states, provides a measure of the validity of the kinetic mechanism. If the spectra of the extracted sequential intermediates do not match those of the model spectra (as is the case for intermediate **4** vs **P**), the mechanism needs to be reevaluated.

The visible spectrum of intermediate **4**, the putative $\mathbf{P_R}$, extracted using a unidirectional sequential mechanism, is pH-dependent (Figure 5), and the spectral differences between pH 8.5 and 6.2 are centered around 595 nm, which corresponds to the absorption peak of compound **A** (*17*). Moreover, when the difference between the spectra of intermediates **4** and **3** (**A**) is analyzed, it shows incomplete conversion of compound **A** to both **P** and **F** (Figure 6). Both these observations suggest that intermediate **4** is a mixture of the **A**, **P**, and **F** spectral components.

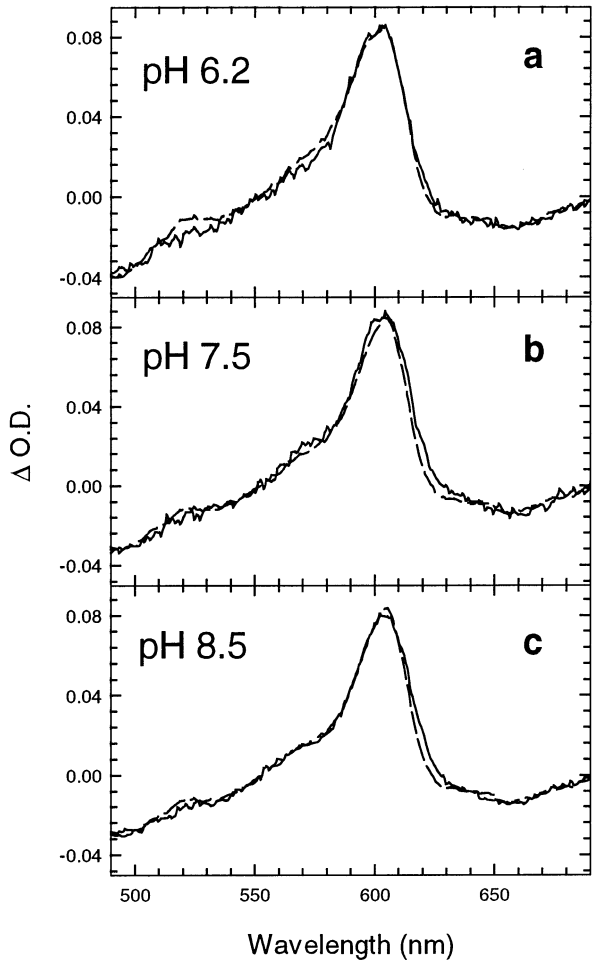

FIGURE 9: Visible experimental spectrum (—) of intermediate **4** ($\mathbf{P_R}$) vs the oxidized enzyme at pH 6.2 (top), 7.5 (middle), and 8.5 (bottom). The difference spectra were extracted from the time-resolved data (Figure 1) using a unidirectional sequential mechanism. A linear combination of the spectrum of compound **A** and the bench-made spectra of **P** ($\mathbf{P_{CO/O_2}}$) and **F** were used to model the data (– – –). The model spectrum of intermediate **4** contains 45% **A** + 5% $\mathbf{P_{CO/O_2}}$ + 50% **F** at pH 6.2, 33% **A** + 34% $\mathbf{P_{CO/O_2}}$ + 33% **F** at pH 7.5, and 30% **A** + 40% $\mathbf{P_{CO/O_2}}$ + 30% **F** at pH 8.5. The oxidized spectrum of Cu_A has been subtracted from the model spectrum to match the redox state of Cu_A in intermediate **4** (Scheme 1).

Figure 9 shows the modeling of intermediate **4**, the putative $\mathbf{P_R}$, at pH 6.2, 7.5, and 8.5 in the visible region by combining the spectra of compound **A**, and the bench-made **P** and **F** in the indicated ratios. The spectra are referenced against the oxidized enzyme. There is an excellent agreement between the spectrum of intermediate **4** (—) and the combination model spectrum (– – –). Interestingly, at pH 6.2 the contribution of **P** is minimal (5%), while compound **A** and **F** contribute roughly equally. On the other hand, at pH 8.5, there are roughly equal contributions of compound **A**, **P**, and **F**. This is consistent with the preferred formation of **P** at alkaline pH values and **F** at acidic pH upon addition of H_2O_2 to the oxidized enzyme (*20*, *39*). The larger contribution of **P** at pH 7.5 and 8.5, compared to that at pH 6.2, is reflected by a significantly higher absorbance between 630 and 650 nm, the red region of the **P** spectrum (Figures 4 and 5). The spectrum of intermediate **4** extracted from the data on the fast enzyme was similarly best represented by a mixture of intermediates.

The Soret spectra of intermediate **4** at the different pHs do not appear to be pH-dependent (Figure 4), contrary to what is observed in the visible region (Figures 4 and 5). The reasons for this are the similarities between the difference spectra of compound **A** (referenced vs the reduced enzyme) and the bench-made **P** and **F** forms (referenced vs the oxidized enzyme) in the Soret region (*24*, *59*, *60*).

The electron transfer between Cu_A and heme *a* is clearly pH-dependent (Figures 7 and 8). The equilibrium is shifted toward oxidized Cu_A and reduced heme *a* ($\mathbf{F_{II}}$) at low pH, which can also be concluded from near-infrared traces published previously (*53*). Previous studies have suggested that the electron transfer is controlled by proton transfer (*32*, *61*−*63*), and the pH dependence of the heme *a*−Cu_A redox equilibrium may reflect a conformational change around the Cu_A site, which could lead to a change in its reduction potential (*64*).

The intermediates of the unidirectional sequential scheme may or may not correspond to a single model spectrum made on the bench. As discussed above, intermediate **1** (**R***), intermediate **2** (**R**), and intermediate **3** (**A**) can be represented by single forms, of which only **R** can be made on the bench. Compound **A** has also been observed during the reaction of the mixed-valence enzyme with dioxygen, and its spectrum is equivalent to that observed for the fully reduced enzyme at room temperature (*17*) and at cryogenic temperatures (*56*−*58*). Intermediate **5** is described well by heme a_3 being in the ferryl state (**F**), with heme *a* and Cu_A sharing the last electron needed to complete the reduction of dioxygen to water.

Intermediate **4** (the putative $\mathbf{P_R}$) could not be modeled with any single bench-made spectrum, and it is different from the corresponding intermediate observed during the reaction of dioxygen with the mixed-valence enzyme, $\mathbf{P_M}$ (*17*). In our first attempt to determine the spectra of the intermediates formed during the reduction of dioxygen to water, the spectrum of intermediate **4** was suggested to be equivalent to the bench-made **P** ($\mathbf{P_{CO/O_2}}$), based on the similarities between their absorption maxima in the visible region (*11*). However, there was a significant difference in the bandwidths between the two spectra, and further experiments in the Soret region revealed large amplitude differences between intermediate **4** and the bench-made **P** form (*24*). To account for these differences, we modeled the spectrum of intermediate **4** in both spectral regions with a ~1:1 mixture of **P** and **F** in a fast equilibrium, with heme *a* remaining reduced in the **P** state and oxidized in the **F** form (*24*). Although the spectrum of intermediate **4** was adequately modeled in the Soret region using this composition, the exact shape in the visible region could not be reproduced.

Sequential Schemes with Back Reactions. The results presented here indicate that intermediate **4** is best represented by a pH-dependent mixture of compound **A**, **P** ($\mathbf{P_M}$), and **F**. The presence of the reduced heme *a* in compound **A** accounts for the large spectral differences in the Soret region observed when intermediate **4** is modeled with pure **P** [Figure 4a (*11*)]. These results indicate that the underlying reaction mechanism of the reduction of dioxygen to water by cytochrome *c* oxidase is more complex than a linear sequence of irreversible steps (Scheme 1). The composition of the intermediates, such as that of intermediate **4** in our unidirectional sequential scheme, can provide important information regarding the

Scheme 2

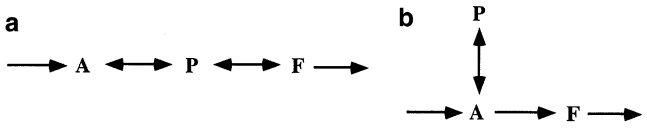

nature of a more appropriate, and more complex, kinetic mechanism. It is well known that the presence of two forms in a sequential intermediate is a sign of either a reversible or a branching step in the underlying reaction mechanism. Using this line of reasoning, the presence of three forms contributing to the sequential intermediate **4** would require two adjacent reversible steps to be introduced into a refined scheme, one between **A** and **P** and one between **P** and **F** (Scheme 2a). Alternatively, intermediate **4** could be formed by branching at **A** to form **P** and **F**, with the conversion of **A** to **P** being reversible (Scheme 2b). We can reject both schemes based on resonance Raman experiments, which have provided evidence that the O−O bond is broken not only in **F** but also in **P** (*16*, *24*−*28*). This would most certainly preclude the back reaction from **P** to **A**. The reversible reaction between **A** and **P** in Scheme 2a would also suggest that intermediate **3** (compound **A**) was a mixture of two spectral forms, which is not observed in our experiments.

A third mechanism involves replacing the sequential scheme with parallel or branched pathways. If the three forms, **A**, **P**, and **F**, are part of two parallel branches overlapping in time, they may be observed simultaneously and would appear as components of a single intermediate in the unidirectional sequential model. The testing of this type of mechanism involves a sophisticated kinetic analysis, which is beyond the scope of this paper, but will be addressed in detail in an accompanying publication.

ACKNOWLEDGMENT

We thank Dr. Guangling Liao for the preparation of the fast enzyme and Dr. John Winterle for technical assistance.

REFERENCES

1. Ferguson-Miller, S., and Babcock, G. T. (1996) *Chem. Rev. 96*, 2889−2907.
2. Zaslavsky, D., and Gennis, R. B. (2000) *Biochim. Biophys. Acta 1458*, 164−179.
3. Varotsis, C., Woodruff, W. H., and Babcock, G. T. (1989) *J. Am. Chem. Soc. 111*, 6439−6440.
4. Ogura, T., Takahashi, S., Shinzawa-Itoh, K., Yoshikawa, S., and Kitagawa, T. (1990) *J. Am. Chem. Soc. 112*, 5630−5631.
5. Han, S., Ching, Y.-C., and Rousseau, D. L. (1990) *Proc. Natl. Acad. Sci. U.S.A. 87*, 2491−2495.
6. Han, S., Ching, Y.-C., and Rousseau, D. L. (1990) *Nature 348*, 89−90.
7. Ogura, T., Takahashi, S., Shinzawa-Itoh, K., Yoshikawa, S., and Kitagawa, T. (1990) *J. Biol. Chem. 265*, 14721−14723.
8. Varotsis, C., Zhang, Y., Appelman, E. H., and Babcock, G. T. (1993) *Proc. Natl. Acad. Sci. U.S.A. 90*, 237−241.
9. Han, S., Takahashi, S., and Rousseau, D. L. (2000) *J. Biol. Chem. 275*, 1910−1919.
10. Morgan, J. E., Verkhovsky, M. I., and Wikström, M. (1996) *Biochemistry 35*, 12235−12240.
11. Sucheta, A., Georgiadis, K. E., and Einarsdóttir, Ó. (1997) *Biochemistry 36*, 554−565.
12. Morgan, J. E., Verkhovsky, M. I., Palmer, G., and Wikström, M. (2001) *Biochemistry 40*, 6882−6892.
13. Proshlyakov, D. A., Ogura, T., Shinzawa-Itoh, K., Yoshikawa, S., Appelman, E. H., and Kitagawa, T. (1994) *J. Biol. Chem. 269*, 29385−29388.
14. Proshlyakov, D. A., Ogura, T., Shinzawa-Itoh, K., Yoshikawa, S., and Kitagawa, T. (1996) *Biochemistry 35*, 76−82.
15. Proshlyakov, D. A., Ogura, T., Shinzawa-Itoh, K., Yoshikawa, S., and Kitagawa, T. (1996) *Biochemistry 35*, 8580−8586.
16. Proshlyakov, D. A., Pressler, M. A., and Babcock, G. T. (1998) *Proc. Natl. Acad. Sci. U.S.A. 95*, 8020−8025.
17. Einarsdóttir, Ó., Szundi, I., Van Eps, N., and Sucheta, A. S. (2002) *J. Inorg. Biochem. 91*, 87−93.
18. Weng, L., and Baker, G. M. (1991) *Biochemistry 30*, 5727−5733.
19. Watmough, N. J., Cheesman, M. R., Greenwood, C., and Thomson, A. J. (1994) *Biochem. J. 300*, 469−475.
20. Fabian, M., and Palmer, G. (1995) *Biochemistry 34*, 13802−13810.
21. Fabian, M., Wong, W. W., Gennis, R. B., and Palmer, G. (1999) *Proc. Natl. Acad. Sci. U.S.A. 96*, 13114−13117.
22. Yoshikawa, S., Shinzawa-Itoh, K., Nakashima, R., Yaono, R., Yamashita, E., Inoue, N., Yao, M., Fei, M. J., Libeu, C. P., Mitzushima, T., Yamaguchi, H., Tomizaki, T., and Tsukihara, T. (1998) *Science 280*, 1723−1731.
23. Ostermeier, C., Harrenga, A., Ermler, U., and Michel, H. (1997) *Proc. Natl. Acad. Sci. U.S.A. 94*, 10547−10553.
24. Sucheta, A., Szundi, I., and Einarsdóttir, Ó. (1998) *Biochemistry 37*, 17905−17914.
25. Gennis, R. B. (1998) *Biochim. Biophys. Acta 1365*, 241−248.
26. Chen, Y. R., Sturgeon, B. E., Gunther, M. R., and Mason, R. P. (1999) *J. Biol. Chem. 274*, 3308−3314.
27. MacMillan, F., Kannt, A., Behr, J., Prisner, T., and Michel, H. (1999) *Biochemistry 38*, 9179−9184.
28. Proshlyakov, D. A., Pressler, M. A., DeMaso, C., Leykam, J. F., DeWitt, D. L., and Babcock, G. T. (2000) *Science 290*, 1588−1591.
29. Iwata, S., Ostermeier, C., Ludwig, B., and Michel, H. (1995) *Nature 376*, 660−669.
30. Tsukihara, T., Aoyama, H., Yamashita, E., Tomizaki, T., Yamaguchi, H., Shinzawa-Itoh, K., Nakashima, R., Yaono, R., and Yoshikawa, S. (1996) *Science 272*, 1136−1144.
31. Konstantinov, A. A., Siletsky, S., Mitchell, D., Kaulen, A., and Gennis, R. B. (1997) *Proc. Natl. Acad. Sci. U.S.A. 94*, 9085−9090.
32. Ädelroth, P., Ek, M. S., Mitchell, D. M., Gennis, R. B., and Brzezinski, P. (1997) *Biochemistry 36*, 13824−13829.
33. Brzezinski, P., and Ädelroth, P. (1998) *J. Bioenerg. Biomembr. 30*, 99−107.
34. Vygodina, T. V., Pecoraro, C., Mitchell, D., Gennis, R., and Konstantinov, A. A. (1998) *Biochemistry 37*, 3053−3061.
35. Zaslavsky, D., and Gennis, R. B. (1998) *Biochemistry 37*, 3062−3067.
36. Bränden, M., Sigurdsson, J., Namslauer, A., Gennis, R. B., Ädelroth, P., and Brzezinski, P. (2001) *Proc. Natl. Acad. Sci. U.S.A. 98*, 5013−5018.
37. Wrigglesworth, J. M. (1984) *Biochem. J. 217*, 715−719.
38. Brittain, T., Little, R. H., Greenwood, C., and Watmough, N. J. (1996) *FEBS Lett. 399*, 21−25.
39. Jünemann, S., Heathcote, P., and Rich, P. R. (2000) *Biochim. Biophys. Acta 1456*, 56−66.
40. Fabian, M., and Palmer, G. (2001) *Biochemistry 40*, 1867−1874.
41. Pecoraro, C., Gennis, R. B., Vygodina, T. V., and Konstantinov, A. A. (2001) *Biochemistry 40*, 9695−9708.
42. Yoshikawa, S., Choc, M. G., O'Toole, M. C., and Caughey, W. S. (1977) *J. Biol. Chem. 252*, 5498−5508.
43. Hartzell, C. R., and Beinert, H. (1974) *Biochim. Biophys. Acta 368*, 318−338.
44. Baker, G. M., Noguchi, M., and Palmer, G. (1987) *J. Biol. Chem. 262*, 595−604.
45. Georgiadis, K. E., Jhon, N.-I., and Einarsdóttir, Ó. (1994) *Biochemistry 33*, 9245−9256.
46. Einarsdóttir, Ó., Georgiadis, K. E., and Sucheta, A. (1995) *Biochemistry 34*, 496−508.
47. Hug, S. J., Lewis, J. W., Einterz, C. M., Thorgeirsson, T. E., and Kliger, D. S. (1990) *Biochemistry 29*, 1475−1485.
48. Thorgeirsson, T. E., Lewis, J. W., Wallace-Williams, S. E., and Kliger, D. S. (1993) *Biochemistry 32*, 13861−13872.
49. Szundi, I., Lewis, J. W., and Kliger, D. S. (1997) *Biophys. J. 73*, 688−702.
50. Slutter, C. E., Sanders, D., Wittung, P., Malmström, B. G., Aasa, R., Richards, J. H., Gray, H. B., and Fee, J. A. (1996) *Biochemistry 35*, 3387−3395.
51. Jasaitis, A., Backgren, C., Morgan, J. E., Puustinen, A., Verkhovsky, M. I., and Wikström, M. (2001) *Biochemistry 40*, 5269−5274.

52. Oliveberg, M., Brzezinski, P., and Malmström, B. G. (1989) *Biochim. Biophys. Acta 977*, 322−328.
53. Hallén, S., and Nilsson, T. (1992) *Biochemistry 31*, 11853−11859.
54. Paula, S., Sucheta, A., Szundi, I., and Einarsdóttir, Ó. (1999) *Biochemistry 38*, 3025−3033.
55. Szundi, I., Liao, G.-L., and Einarsdóttir, Ó. (2001) *Biochemistry 40*, 2332−2339.
56. Chance, B., Saronio, C., and Leigh, J. S., Jr. (1975) *J. Biol. Chem. 250*, 9226−9237.
57. Clore, M. G., Andréasson, L.-E., Karlsson, B. G., Aasa, R., and Malmström, B. (1980) *Biochem. J. 185*, 139−154.
58. Clore, M. G., Andréasson, L.-E., Karlsson, B. G., Aasa, R., and Malmström, B. (1980) *Biochem. J. 185*, 155−167.
59. Denis, M. (1981) *Biochim. Biophys. Acta 634*, 30−40.
60. Fabian, M., and Palmer, G. (1995) *Biochemistry 34*, 1534−1540.
61. Hallén, S., Brzezinski, P., and Malmström, B. G. (1994) *Biochemistry 33*, 1467−1472.
62. Karpefors, M., Ädelroth, P., Zhen, Y., Ferguson-Miller, S., and Brzezinski, P. (1998) *Proc. Natl. Acad. Sci. U.S.A. 95*, 13606−13611.
63. Ädelroth, P., Karpefors, M., Gilderson, G., Tomson, F. L., Gennis, R. B., and Brzezinski, P. (2000) *Biochim. Biophys. Acta 1459*, 533−539.
64. Gupta, S., Warne, A., Saraste, M., and Mazumdar, S. (2001) *Biochemistry 40*, 6180−6189.

BI020482M